

The Light Higgsino-dominated NLSPs in the Semi-constrained NMSSM^{*}

Kun Wang^{1;1)} Jingya Zhu^{1;2)}

¹ Center for Theoretical Physics, School of Physics and Technology, Wuhan University, Wuhan 430072, China

Abstract: In the semi-constrained NMSSM (scNMSSM, or NMSSM with non-universal Higgs mass) under current constraints, we consider a scenario where h_2 is the SM-like Higgs, $\tilde{\chi}_1^0$ is singlino-dominated LSP, $\tilde{\chi}_1^\pm$ and $\tilde{\chi}_2^0, \tilde{\chi}_3^0$ are mass-degenerated, light and higgsino-dominated NLSPs (next-to-lightest supersymmetric particles). We investigate the constraints to these NLSPs from searching for SUSY particles at the LHC Run-I and Run-II, discuss the possibility of discovering these NLSPs in the future, and come to the following conclusions: (i) With all data of Run I and up to 36 fb^{-1} data of Run II at the LHC, the search results by ATLAS and CMS can still not exclude the higgsino-dominated NLSPs of $100 \sim 200 \text{ GeV}$. (ii) When the mass difference with $\tilde{\chi}_1^0$ is smaller than m_{h_2} , $\tilde{\chi}_2^0$ and $\tilde{\chi}_3^0$ have opposite preference on decaying to Z/Z^* or h_1 . (iii) When the mass difference between NLSP and LSP is larger than m_Z , most of the samples can be checked at 5σ level with future 300 fb^{-1} data at the LHC. While with 3000 fb^{-1} data at the High Luminosity LHC (HL-LHC), nearly all of the samples can be checked at 5σ level even if the mass difference is insufficient. (iv) The a_1 funnel and the h_2/Z funnel mechanisms for the singlino-dominated LSP annihilating can not be distinguished by searching for NLSPs.

Keywords: NMSSM, supersymmetry phenomenology, higgsino

PACS: 11.30 Pb **DOI:** 10.1088/1674-1137/44/xx/xxxxxx

1 Introduction

As an internal symmetry between fermions and bosons, Supersymmetry (SUSY) is an attractive idea. In the framework of SUSY, the strong, weak and hypercharge gauge couplings (g_3, g_2, g_1) can be unified at the GUT scale ($\sim 10^{16} \text{ GeV}$), and the large hierarchy problem between the electroweak scale and the Planck scale can be solved. Besides, with the R-parity conserved, the lightest SUSY particle (LSP) is stable and can be a good candidate for weakly-interaction-massive-particle (WIMP) dark matter (DM).

SUSY at TeV scale is motivated by the possible cancellation of quadratic divergences of the Higgs boson mass. And the simplest implementation of SUSY is the Minimal Supersymmetric extension to the Standard Model (MSSM). Since the soft SUSY breaking parameters is totally free in the MSSM, a dynamic way to get these parameters is more favored. In the minimal supergravity (mSUGRA), the Käler potential is employed to yield the minimal kinetic energy terms for the MSSM fields, where all the trilinear couplings, gaugino, and scalar mass parameters unify respectively at the GUT

scale. The fully constrained MSSM (CMSSM) is the MSSM with the boundary conditions the same as the mSUGRA. But to get a 125 GeV SM-like Higgs, the MSSM needs very large one-loop radiative corrections to Higgs mass, which makes the MSSM not natural. And there is a so-called μ -problem [1] in the MSSM, where the superpotential contains a term $\mu \hat{H}_u \hat{H}_d$, and μ is the only dimensionful parameter and has to be chosen artificially.

The Next-to Minimal Supersymmetric Standard Model (NMSSM) can solve the μ -problem by introducing a complex singlet superfield \hat{S} , which can generate an effective μ -term dynamically. And it can easily predict an SM-like 125 GeV Higgs, under all the constraints and with low fine-tuning [2]. The fully constrained NMSSM (cNMSSM) contains none or only one more parameter than the CMSSM/mSUGRA, thus both of them are in tension with current experimental constraints including 125 GeV Higgs mass, high mass bound of gluino, muon g-2, and dark matter [3–8]. So, we consider the semi-constrained NMSSM (scNMSSM), which relaxes the unification of scalar masses by decoupling the squared-masses of the Higgs bosons and the squarks/sleptons, which is also called NMSSM with non-universal Higgs

Accepted 24 Feb 2020

* supported by the National Natural Science Foundation of China (NNSFC) under grant Nos. 11605123.

1) E-mail: wk2016@whu.edu.cn

2) E-mail: zhuyj@whu.edu.cn

©2020 Chinese Physical Society and the Institute of High Energy Physics of the Chinese Academy of Sciences and the Institute of Modern Physics of the Chinese Academy of Sciences and IOP Publishing Ltd

mass (NUHM) [9–11]. In the scNMSSM, the bino and wino are heavy because the high mass bound of gluino and the unification of gaugino masses at GUT scale, thus the light neutralinos and charginos can only be singlino-dominated or higgsino-dominated¹⁾.

In recent years, the ATLAS and CMS collaborations have carried out many searches for SUSY particles, which pushed the gluino and squarks masses bounds in simple models up to several hundred GeV and even TeV scale. While it is still possible for the electroweakino sector to be very light. The electroweakino sector of NMSSM was studied in [12–18], among which different search channels were provided, such as multi-leptons [15, 16], and jets with missing transverse momentum (\cancel{p}_T) [17]. These motivated us to check the current status of higgsino, in special SUSY models such as the scNMSSM, under direct-search constraints and their possibility of discovery by detailed simulation.

In this work, we discuss the light higgsino-dominated NLSPs (next-to-lightest supersymmetric particles) in the scNMSSM. We use the scenario of singlino-dominated $\tilde{\chi}_1^0$ and SM-like h_2 in the scan result in our former work on scNMSSM [11], where we considered the constraints including theoretical constraints of vacuum stability and Landau pole, experimental constraints of Higgs data, muon g-2, B physics, dark matter relic density and direct searches, etc. Thus in this scenario the $\tilde{\chi}_1^\pm$ and $\tilde{\chi}_{2,3}^0$ are higgsino-dominated, light and mass-degenerated NLSPs. We first investigate the constraints to these NLSPs, including searching for SUSY particle at the LHC Run-I and Run-II. We use Monte Carlo to do the detailed simulations to impose these constraints. Then we discuss the possibility of discovering the higgsino-dominated NLSPs in the future at the High Luminosity LHC (HL-LHC).

This paper is organized as follows. First, in Section 2, we briefly introduce the model of NMSSM and scNMSSM, especially the Higgs and electroweakino sector. Later in Section 3, we discuss the constraints to the light higgsino-dominated NLSPs, and the possibility of discovering them at the HL-LHC. Finally, we draw our conclusions in Section 4.

2 Introduction to the NMSSM and scNMSSM

The superpotential of NMSSM with \mathbb{Z}_3 symmetry :

$$W_{\text{NMSSM}} = W_{\text{MSSM}}|_{\mu=0} + \lambda \hat{S} \hat{H}_u \cdot \hat{H}_d + \frac{\kappa}{3} \hat{S}^3, \quad (1)$$

where the superfields \hat{H}_u and \hat{H}_d are two complex doublet superfields, the superfield \hat{S} is the singlet superfield, the coupling constants λ and κ are dimensionless, and

1) The behaviors of the cNMSSM under recent constraints is similar as the CMSSM, where the additional parameter λ is very small, and higgsino mass parameter μ_{eff} is calculated to be very large, thus the higgsino-dominated and singlino-dominated neutralinos are very heavy [7, 8].

the $W_{\text{MSSM}}|_{\mu=0}$ is actually the Yukawa couplings of the \hat{H}_u and \hat{H}_d to the quark and lepton superfields. When electroweak symmetry breaking, the scalar component of superfields \hat{H}_u , \hat{H}_d and \hat{S} get their vacuum expectation values (VEVs) v_u , v_d and v_s respectively. The relations between the VEVs are

$$\tan\beta = v_u/v_d, \quad v = \sqrt{v_u^2 + v_d^2} = 174 \text{ GeV}, \quad \mu_{\text{eff}} = \lambda v_s, \quad (2)$$

where the μ_{eff} is the mass scale of higgsino, like in the MSSM. In the following, for the sake of convenience, we refer to μ_{eff} as μ .

The soft SUSY breaking terms in the NMSSM is only different from the MSSM in several terms:

$$-\mathcal{L}_{\text{NMSSM}}^{\text{soft}} = -\mathcal{L}_{\text{MSSM}}^{\text{soft}}|_{\mu=0} + m_S^2 |S|^2 + \lambda A_\lambda S H_u \cdot H_d + \frac{1}{3} \kappa A_\kappa S^3 + h.c., \quad (3)$$

where the S , H_u and H_d is the scalar component of the superfields, the m_S^2 is the soft SUSY breaking mass for singlet field S , and the trilinear coupling constants A_λ and A_κ have mass dimension.

In the semi-constrained NMSSM (scNMSSM), the Higgs sector are considered non-universal, that is, the Higgs soft mass $m_{H_u}^2$, $m_{H_d}^2$ and m_S^2 are allowed to be different from $M_0^2 + \mu^2$, and the trilinear couplings A_λ , A_κ can be different from A_0 . Hence, in the scNMSSM, the complete parameter sector is usually chosen as:

$$\lambda, \kappa, \tan\beta, \mu, A_\lambda, A_\kappa, A_0, M_{1/2}, M_0. \quad (4)$$

2.1 The Higgs sector of NMSSM and scNMSSM

When the electroweak symmetry breaking, the scalar component of superfields \hat{H}_u , \hat{H}_d and \hat{S} can be written as

$$H_u = \begin{pmatrix} H_u^+ \\ v_u + \frac{H_u^R + i H_u^I}{\sqrt{2}} \end{pmatrix}, \quad H_d = \begin{pmatrix} v_d + \frac{H_d^R + i H_d^I}{\sqrt{2}} \\ H_d^- \end{pmatrix}, \quad S = v_s + \frac{S^R + i S^I}{\sqrt{2}}, \quad (5)$$

where H_u^R , H_d^R , and S^R are CP-even component fields, H_u^I , H_d^I , and S^I are the CP-odd component fields, and the H_u^+ and H_d^- are charged component fields

In the basis (H_d^R, H_u^R, S^R) , the CP-even scalar mass matrix is [19]

$$\mathcal{L} \ni \frac{1}{2} (H_d^R, H_u^R, S^R) M_S^2 \begin{pmatrix} H_d^R \\ H_u^R \\ S^R \end{pmatrix} \quad (6)$$

with

$$M_S^2 = \begin{pmatrix} M_A^2 s_\beta^2 + M_Z^2 c_\beta^2 & (2\lambda v^2 - M_A^2 - M_Z^2) s_\beta c_\beta & C c_\beta + C' s_\beta \\ (2\lambda v^2 - M_A^2 - M_Z^2) s_\beta c_\beta & M_A^2 c_\beta^2 + M_Z^2 s_\beta^2 & C s_\beta + C' c_\beta \\ C c_\beta + C' s_\beta & C s_\beta + C' c_\beta & M_{S, S^R S^R}^2 \end{pmatrix} \quad (7)$$

where

$$M_A^2 = \frac{2\mu(A_\lambda + \kappa v_s)}{\sin 2\beta}, \quad (8)$$

$$C = 2\lambda^2 v v_s, \quad C' = \lambda v (A_\lambda - 2\kappa v_s), \quad (9)$$

$$M_{S, S^R S^R}^2 = \lambda A_\lambda \frac{v_u v_d}{v_s} + \kappa v_s (A_\kappa + 4\kappa v_s), \quad (10)$$

and $s_\beta = \sin \beta, c_\beta = \cos \beta$. Actually, there is a more common basis (H_1, H_2, S^R) , where

$$H_1 = H_u^R c_\beta - H_d^R s_\beta, \quad H_2 = H_u^R s_\beta + H_d^R c_\beta \quad (11)$$

and the H_2 is the SM Higgs field. In the basis (H_1, H_2, S^R) , the scalar mass matrix is different from Eq.(7). But, since the rotation of the basis do not touch the third component S^R , the $M_{S, S^R S^R}^2$ will keep the same as in Eq.(10). The Higgs boson mass matrix M_S^2 in basis (H_1, H_2, S^R) is given by [20]

$$M_{S', H_1 H_1}^2 = M_A^2 + (m_Z^2 - \lambda^2 v^2) \sin^2 2\beta, \quad (12)$$

$$M_{S', H_1 H_2}^2 = -\frac{1}{2} (m_Z^2 - \lambda^2 v^2) \sin 4\beta, \quad (13)$$

$$M_{S', H_1 S^R}^2 = -\left(\frac{M_A^2}{2\mu/\sin 2\beta} + \kappa v_s \right) \lambda v \cos 2\beta, \quad (14)$$

$$M_{S', H_2 H_2}^2 = m_Z^2 \cos^2 2\beta + \lambda^2 v^2 \sin^2 2\beta, \quad (15)$$

$$M_{S', H_2 S^R}^2 = 2\lambda\mu v \left[1 - \left(\frac{M_A}{2\mu/\sin 2\beta} \right)^2 - \frac{\kappa}{2\lambda} \sin 2\beta \right], \quad (16)$$

$$M_{S', S^R S^R}^2 = \frac{1}{4} \lambda^2 v^2 \left(\frac{M_A}{\mu/\sin 2\beta} \right)^2 + \kappa v_s A_\kappa + 4(\kappa v_s)^2 - \frac{1}{2} \lambda \kappa v^2 \sin 2\beta. \quad (17)$$

And comparing Eq.(17) with Eq.(10), it's not hard to get $M_{S', S^R S^R}^2 = M_{S, S^R S^R}^2$.

To get the physical CP-odd scalar Higgs bosons, one can rotate the Higgs fields,

$$A = H_u^I c_\beta + H_d^I s_\beta. \quad (18)$$

Then the Goldstone mode can be dropped off, and the CP-odd scalar mass matrix in the basis (A, S^I) become [19]

$$\mathcal{L} \ni \frac{1}{2} (A, S^I) M_P^2 \begin{pmatrix} A \\ S^I \end{pmatrix} \quad (19)$$

with

$$M_P^2 = \begin{pmatrix} M_A^2 & \lambda v (A_\lambda - 2\kappa v_s) \\ \lambda v (A_\lambda - 2\kappa v_s) & M_{P, S^I S^I}^2 \end{pmatrix} \quad (20)$$

where

$$M_{P, S^I S^I}^2 = \lambda (A_\lambda + 4\kappa v_s) \frac{v_u v_d}{v_s} - 3\kappa v_s A_\kappa. \quad (21)$$

The mass eigenstates of the CP-even Higgs h_i ($i = 1, 2, 3$) and the CP-odd Higgs A_i ($i = 1, 2$) can be obtained

by

$$\begin{pmatrix} h_1 \\ h_2 \\ h_3 \end{pmatrix} = S_{ij} \begin{pmatrix} H_1 \\ H_2 \\ S^R \end{pmatrix}, \quad \begin{pmatrix} a_1 \\ a_2 \end{pmatrix} = P_{ij} \begin{pmatrix} A \\ S^I \end{pmatrix}, \quad (22)$$

where the matrix S_{ij} can diagonalize the mass matrix $M_{S'}^2$, and the matrix P_{ij} can diagonalize the mass matrix M_P^2 .

2.2 The electroweakino sector of NMSSM and scNMSSM

In the NMSSM, there are five neutralinos $\tilde{\chi}_i^0$ ($i = 1, 2, 3, 4, 5$), which are the mixture of \tilde{B} (bino), \tilde{W}^3 (wino), \tilde{H}_d^0 , \tilde{H}_u^0 (higgsinos) and \tilde{S} (singlino). In the gauge-eigenstate basis $\psi^0 = (\tilde{B}, \tilde{W}^3, \tilde{H}_d^0, \tilde{H}_u^0, \tilde{S})$, the neutralino mass matrix takes the form [19]

$$M_{\tilde{\chi}^0} = \begin{pmatrix} M_1 & 0 & -c_\beta s_W m_Z & s_\beta s_W m_Z & 0 \\ 0 & M_2 & c_\beta c_w m_z & -s_\beta c_w m_Z & 0 \\ -c_\beta s_W m_Z & c_\beta c_w m_z & 0 & -\mu & -\lambda v_d \\ s_\beta s_W m_Z & -s_\beta c_w m_Z & -\mu & 0 & -\lambda v_u \\ 0 & 0 & -\lambda v_d & -\lambda v_u & 2\kappa v_s \end{pmatrix} \quad (23)$$

where $s_\beta = \sin \beta, c_\beta = \cos \beta, s_W = \sin \theta_W, c_W = \cos \theta_W$. To get the mass eigenstates, one can diagonalize the neutralino mass matrix $M_{\tilde{\chi}^0}$

$$N^* M_{\tilde{\chi}^0} N^{-1} = M_{\tilde{\chi}^0}^D = \text{Diag}(m_{\tilde{\chi}_1^0}, m_{\tilde{\chi}_2^0}, m_{\tilde{\chi}_3^0}, m_{\tilde{\chi}_4^0}, m_{\tilde{\chi}_5^0}) \quad (24)$$

where $M_{\tilde{\chi}^0}^D$ means the diagonal mass matrix, and the order of eigenvalues is $m_{\tilde{\chi}_1^0} < m_{\tilde{\chi}_2^0} < m_{\tilde{\chi}_3^0} < m_{\tilde{\chi}_4^0} < m_{\tilde{\chi}_5^0}$. Meanwhile, one can get the mass eigenstates

$$\begin{pmatrix} \tilde{\chi}_1^0 \\ \tilde{\chi}_2^0 \\ \tilde{\chi}_3^0 \\ \tilde{\chi}_4^0 \\ \tilde{\chi}_5^0 \end{pmatrix} = N_{ij} \begin{pmatrix} \tilde{B} \\ \tilde{W}^0 \\ \tilde{H}_d \\ \tilde{H}_u \\ \tilde{S} \end{pmatrix} \quad (25)$$

In the scNMSSM, bino and wino were constrained to be very heavy, because of the high mass bounds of gluino and the universal gaugino mass at the GUT scale, thus they can be decoupled from the light sector. Then the following relations for the N_{ij} can be found [21]:

$$N_{i3} : N_{i4} : N_{i5} = \left[\frac{m_{\tilde{\chi}_i^0}}{\mu} s_\beta - c_\beta \right] : \left[\frac{m_{\tilde{\chi}_i^0}}{\mu} c_\beta - s_\beta \right] : \frac{\mu - m_{\tilde{\chi}_i^0}}{\lambda v} \quad (26)$$

We assume the lightest neutralino $\tilde{\chi}_1^0$ is the lightest supersymmetric particle (LSP) and makes up of the cosmic dark matter. If the LSP $\tilde{\chi}_1^0$ satisfies $N_{15}^2 > 0.5$, we call it singlino-dominated. And the coupling of such an

LSP with the CP-even Higgs bosons is given by [21]

$$C_{h_1\tilde{\chi}_1^0\tilde{\chi}_1^0} = \sqrt{2}\lambda \left[S_{i1}N_{15}(N_{13}c_\beta - N_{14}s_\beta) + S_{i2}N_{15}(N_{14}c_\beta + N_{13}s_\beta) + S_{i3}(N_{13}N_{14} - \frac{\kappa}{\lambda}N_{15}^2) \right] \quad (27)$$

In the singlino-dominated-LSP scenario, taken $N_{11} = N_{12} = 0$, the mass of LSP can be written as $m_{\tilde{\chi}_1^0} \approx M_{\tilde{\chi}_1^0, \tilde{S}\tilde{S}} = 2\kappa v_s$. And from Eq.(23), Eq.(10) and Eq.(21), one can find the sum rule [22]:

$$M_{\tilde{\chi}_1^0, \tilde{S}\tilde{S}}^2 = 4\kappa^2 v_s^2 = M_{S, SRSR}^2 + \frac{1}{3}M_{P, SISI}^2 - \frac{4}{3}v_u v_d \left(\frac{\lambda^2 A_\lambda}{\mu} + \kappa \right) \quad (28)$$

In the case that h_1 singlet-like, $\tan\beta$ sizable, λ, κ and A_λ not too large, this equation can become

$$m_{\tilde{\chi}_1^0}^2 \approx m_{h_1}^2 + \frac{1}{3}m_{a_1}^2 \quad (29)$$

The chargino sector in the NMSSM is similar to neutralino sector. The charged higgsino \tilde{H}_u^+ , \tilde{H}_d^- (with mass scale μ) and the charged gaugino \tilde{W}^\pm (with mass scale M_2) can also mix respectively, forming two couples of physical chargino $\tilde{\chi}_1^\pm, \tilde{\chi}_2^\pm$. In the gauge-eigenstate basis $(\tilde{W}^+, \tilde{H}_u^+, \tilde{W}^-, \tilde{H}_d^-)$, the chargino mass matrix is given by [19]

$$M_{\tilde{C}} = \begin{pmatrix} 0 & X^T \\ X & 0 \end{pmatrix}, \quad \text{where } X = \begin{pmatrix} M_2 & \sqrt{2}s_\beta m_W \\ \sqrt{2}c_\beta m_W & \mu \end{pmatrix} \quad (30)$$

To obtain the chargino mass eigenstates, one can use two unitary matrix to diagonalize the chargino mass matrix by

$$U^* X V^{-1} = M_{\tilde{\chi}^\pm}^D = \text{Diag}(m_{\tilde{\chi}_1^\pm}, m_{\tilde{\chi}_2^\pm}) \quad (31)$$

where $M_{\tilde{\chi}^\pm}^D$ means the diagonal mass matrix, and the order of eigenvalues is $m_{\tilde{\chi}_1^\pm} < m_{\tilde{\chi}_2^\pm}$. Meanwhile, we can get the mass eigenstates

$$\begin{pmatrix} \tilde{\chi}_1^+ \\ \tilde{\chi}_2^+ \end{pmatrix} = V_{ij} \begin{pmatrix} \tilde{W}^+ \\ \tilde{H}_u^+ \end{pmatrix}, \quad \begin{pmatrix} \tilde{\chi}_1^- \\ \tilde{\chi}_2^- \end{pmatrix} = U_{ij} \begin{pmatrix} \tilde{W}^- \\ \tilde{H}_d^- \end{pmatrix}. \quad (32)$$

In the scNMSSM, since $M_2 \gg \mu$, $\tilde{\chi}_1^\pm$ can be higgsino-dominated, with mass around μ . With $\tilde{\chi}_1^0$ singlino-dominated, $\tilde{\chi}_{2,3}^0$ can be higgsino-dominated, with masses nearly degenerate also around μ , and with $N_{23}^2 + N_{24}^2 > 0.5$. Then with μ not large, smaller than other sparticle mass, the nearly-degenerate $\tilde{\chi}_1^\pm$ and $\tilde{\chi}_{2,3}^0$ can be called the next-to-lightest SUSY particles (NLSPs). In this work, we will focus on the detection of the higgsino-dominated NLSPs ($\tilde{\chi}_1^\pm$ and $\tilde{\chi}_{2,3}^0$) in the scNMSSM.

2) The detail of the constraints can be found in Ref.[11]. For the dark matter relic density, we only consider the upper bound, that is $\Omega h^2 \leq 0.131$, considering there may be also other sources of dark matter.

3 The Light Higgsino-dominated NLSPs in scNMSSM

In this work, we use the scan result in our former work on scNMSSM [11], but only consider the surviving samples with singlino-dominated $\tilde{\chi}_1^0$ ($|N_{15}|^2 > 0.5$) as the LSP, and impose the SUSY search constraints with CheckMATE [23]. We did the scan with the program NMSSMTools-5.4.1 [24], and considered the constraints there, including theoretical constraints of vacuum stability and Landau pole, experimental constraints of Higgs data, muon g-2, B physics, dark matter relic density and direct searches, etc²⁾. We also use HiggsBounds-5.1.1beta [25] to constrain the Higgs sector (with h_2 as the SM-like Higgs and $123 < m_{h_2} < 127$ GeV), and SModelS-v1.1.1 [26] to constrain the SUSY particles. The scanned spaces of the parameters are:

$$\begin{aligned} 0 < M_0 < 500 \text{ GeV}, 0 < M_{1/2} < 2 \text{ TeV}, |A_0| < 10 \text{ TeV}, \\ 100 < \mu < 200 \text{ GeV}, 1 < \tan\beta < 30, 0.3 < \lambda < 0.7, \\ 0 < \kappa < 0.7, |A_\lambda| < 10 \text{ TeV}, |A_\kappa| < 10 \text{ TeV}. \end{aligned} \quad (33)$$

As shown in Ref.[11], in the survived parameter space,

- Glugino is heavier than 1.5 TeV, thus $M_{1/2}$ at GUT scale, or $M_3/2.4 \simeq M_2/0.8 \simeq M_1/0.4$ at M_{SUSY} scale due to RGE runnings, is larger than about 700 GeV.
- Due to the RGE runnings including M_3 , the squarks can be heavy. Even the lightest squarks, e.g. \tilde{t}_1 , are heavier than about 500 GeV.
- Due to the RGE runnings including M_2 and M_1 , the sleptons of the first two generations and all sneutrinos are heavier than about 300 GeV, only the $\tilde{\tau}_1$ can be lighter than that and to about 100 GeV.
- The heavy charginos $\tilde{\chi}_2^\pm$ are wino-like and heavier than about 560 GeV, the light charginos $\tilde{\chi}_1^\pm$ are higgsino-like at 100~200 GeV.
- For the five neutralinos, $\tilde{\chi}_5^0$ is wino-like and heavier than 560 GeV, the bino-dominated neutralino is heavier than 280 GeV, the higgsino-dominated neutralinos are 100~200 GeV, while the singlino-dominated neutralino can be 60~400 GeV.
- For the Higgs sector, h_2 is the SM-like Higgs at $123 \sim 127$ GeV, h_1 is singlet-dominated and lighter than 123 GeV, the light CP-odd Higgs is singlet-dominated but can be lighter or heavier than 125 GeV. Since h_2 is SM-like, the Higgs invisible decay caused by $m_{\tilde{\chi}_1^0} \simeq 60$ GeV is at most

about 20%, so as the Higgs exotic decays caused by $m_{h_1,a_1} \lesssim 60$ GeV.

In this work, we choose the survived samples with $\tilde{\chi}_1^0$ LSP as singlino-dominated, and higgsino-dominated neutralino and chargino ($\tilde{\chi}_1^\pm$ and $\tilde{\chi}_{2,3}^0$) as NLSPs. Thus the samples with higgsino-dominated neutralino as LSP, or $\tilde{\tau}_1$ as NLSP, are discarded. In the following, we focus on the higgsino-dominated NLSPs in the scNMSSM, considering its constraints from direct search results at the LHC Run I and Run II, its production and decay, and its possibility of discovery at the HL-LHC in the future.

3.1 Constraints from Direct SUSY Searches with CheckMATE

In this work, we besides use CheckMATE 2.0.26 [23] to impose these constraints of direct SUSY search results at the LHC, which using all data at Run I and up to 36 fb^{-1} data at Run II [27–30]. With masses at $100 \sim 200$ GeV, the cross sections of the higgsino-dominated NLSPs can be sizeable, thus we pay special attention to the NLSPs.

Firstly, We use `MadGraph5_aMC@NLO 2.6.6`[31] to generate three types of tree level processes at 8 TeV and 13 TeV:

$$pp \rightarrow \tilde{\chi}_1^+ \tilde{\chi}_1^-, \quad pp \rightarrow \tilde{\chi}_1^\pm \tilde{\chi}_{2,3}^0, \quad pp \rightarrow \tilde{\chi}_{2,3}^0 \tilde{\chi}_{2,3}^0. \quad (34)$$

Since the cross sections by the `MadGraph` are at tree level, we multiply them by a NLO K-factor calculated with the `Prospino2` [32]. Then, we use the `PYTHIA 8.2` [33] to deal with particle decay, parton showering, and hardronization, use `Delphes 3.4.1` [34] to simulate the detector response, and use the anti- k_T algorithm [35] for jet clustering.

After the simulation, we can get a ‘.root’ file. We use the `CheckMATE2` to read this ‘.root’ file. Then, we apply the same cuts in signal regions of the CMS and ATLAS experiments at 8 TeV and 13 TeV, by using analysis cards which have been implemented in `CheckMATE2`. At the last step, with the `CheckMATE2` we get a r -value for each samples, which is defined as

$$r \equiv \frac{S - 1.64\Delta S}{S_{Exp.}^{95}} \quad (35)$$

where S is the total number of expected signal events, ΔS is the uncertainty of S , and $S_{Exp.}^{95}$ is the experimentally measured 95% confidence limit of signal events number. So, a model can be considered excluded at 95% confidence level, if $r \geq 1$. If the $r \geq 1$ in only one signal region, the model can also be excluded. We can get r_{max} ,

the maximal value of r in different signal regions. The model is excluded if $r_{max} \geq 1$.

After using `CheckMATE` to checking our surviving samples, we notice that most of the samples excluded are by the CMS analysis in multilepton final states at 13 TeV LHC with 35.9 fb^{-1} data [27]³⁾. We checked that the relevant mechanism is $\tilde{\chi}_1^\pm \tilde{\chi}_2^0$ produced and each decaying to 2 bodies. Since the sleptons are heavier, the $\tilde{\chi}_1^\pm$ and $\tilde{\chi}_2^0$ mainly decay to the $\tilde{\chi}_1^0$ LSP plus a W , or Z , or Higgs boson. The most effective processes excluding the samples are $pp \rightarrow \tilde{\chi}_1^\pm (W^\pm \tilde{\chi}_1^0) \tilde{\chi}_2^0 (Z \tilde{\chi}_1^0)$ and $pp \rightarrow \tilde{\chi}_1^\pm (W^\pm \tilde{\chi}_1^0) \tilde{\chi}_2^0 (h_2 \tilde{\chi}_1^0)$.

The searching strategy for these two processes is three or more leptons plus large \not{p}_T in the final state, since these channels are relatively cleaner than the jet channels at the LHC. The CMS searches related to our processes included the following signal regions (SR) SR-A, SR-C and SR-F

- **SR-A:** events with three light leptons (e or μ), two of which forming an opposite sign same-flavor (OSSF) pair. The SR-A is divided into 44 bins, according to the invariant mass of OSSF pair $M_{\ell\ell}$, the third lepton’s transverse mass M_T and the missing transverse momentum \not{p}_T . The transverse mass M_T is defined as

$$M_T = \sqrt{2p_T^\ell \not{p}_T [1 - \cos(\Delta\phi)]}, \quad (36)$$

where $\Delta\phi$ is the angle between \not{p}_T^ℓ and \not{p}_T .

- **SR-C:** events with two light leptons (e or μ) forming an OSSF pair, and one τ_h candidate. The SR-C is divided into 18 bins, according to the invariant mass $M_{\ell\ell}$, the two-lepton ‘stransverse mass’ $M_{T2}(\ell_1, \ell_2)$ [37] instead of M_T on the off-Z regions, and the \not{p}_T . The M_{T2} is defined as

$$M_{T2} = \min_{\not{p}_T^1 + \not{p}_T^2 = \not{p}_T} [\max \{M_T(\not{p}_T^{\ell_1}, \not{p}_T^1), M_T(\not{p}_T^{\ell_2}, \not{p}_T^2)\}], \quad (37)$$

where $\not{p}_T^{\ell_1}$ and $\not{p}_T^{\ell_2}$ are the transverse momentum for the two leptons respectively, while \not{p}_T^1 and \not{p}_T^2 stand for the random two components of the missing transverse momentum \not{p}_T . And it is used to suppressed the SM background, since the large $t\bar{t}$ background is at low M_{T2} .

- **SR-F:** events with one light lepton (e or μ) plus two τ_h candidates. SR-F is divided into 12 bins, according to $M_{\ell\ell}$, $M_{T2}(\ell, \tau_1)$ and the \not{p}_T .

Recently after 2017, ATLAS and CMS collaborations have released several new search results with more Run-

3) The CMS collaboration has not released update results with more data in the multilepton channel up to now. The cut scheme of ATLAS analysis in this channel is different, and we checked that the ATLAS result with 13.3 fb^{-1} data [28] implemented in the `CheckMATE` is much weaker than the CMS result in constraining our samples, and thus even with 139 fb^{-1} data [36] it has no significant impact on our final conclusion. We also have considered the CMS analysis for the compressed spectrum with 12.9 fb^{-1} data [29], and find that even with the current 139 fb^{-1} data it can not constrain our samples more.

II data up to 139 fb^{-1} in such channels as $2\ell+\not{p}_T$ [38], $3\ell+\not{p}_T$ [36] (see also non-SUSY interpretations of multilepton anomalies in Refs.[39]), $2\gamma+\not{p}_T$ [40], Higgs+ \not{p}_T [41], and Higgs+ $\ell+\not{p}_T$ [42], and for compressed mass spectrum [43]. In their analyses, they considered simple models, where purely higgsino or wino NLSP produced in pair, each decaying to $\tilde{\chi}_1^0$ plus h , Z , or W^\pm in 100%, so the results do not apply to our samples directly. Imposing these new constraints is fussy, so we tend to put them in our later works.

3.2 Production and decay of the higgsino-dominated NLSPs

For the surviving samples we first checked the production cross sections of $\tilde{\chi}_1^+\tilde{\chi}_2^0$, $\tilde{\chi}_1^+\tilde{\chi}_3^0$, $\tilde{\chi}_1^-\tilde{\chi}_2^0$, $\tilde{\chi}_1^-\tilde{\chi}_3^0$, $\tilde{\chi}_1^+\tilde{\chi}_1^-$, $\tilde{\chi}_2^0\tilde{\chi}_3^0$, $\tilde{\chi}_2^0\tilde{\chi}_2^0$ and $\tilde{\chi}_3^0\tilde{\chi}_3^0$ at the 14 TeV LHC. Since the NLSPs are higgsino-dominated, the cross sections are not much different from those of pure higgsino production. Here we only revise some of the old conclusions.

- The cross sections reduce quickly when the masses increasing, for the partonic Mandelstam variable \hat{s} increase, and the parton fluxes decrease.
- The cross section of $\tilde{\chi}_1^+\tilde{\chi}_i^0$ is about 2 times of $\tilde{\chi}_1^-\tilde{\chi}_i^0$, for both $i=2$ and 3. The reason is that the LHC is proton-proton collider, and the parton distribution functions (PDF) for up quark is larger than down quark.
- The cross sections of $\tilde{\chi}_2^0\tilde{\chi}_2^0$ and $\tilde{\chi}_3^0\tilde{\chi}_3^0$ are very small, only a few fb. The reason is that the squarks are very heavy, so $pp\rightarrow\tilde{\chi}_i^0\tilde{\chi}_i^0$ are mainly produced from s channel through Z boson resonance. The coupling of $Z-\tilde{\chi}_i^0-\tilde{\chi}_i^0$ is given by

$$C_{Z\tilde{\chi}_i^0\tilde{\chi}_j^0} = -\frac{i}{2}(g_1 s_W + g_2 c_W)(N_{j3}^* N_{i3} - N_{j4}^* N_{i4})(\gamma_\mu P_L) + \frac{i}{2}(g_1 s_W + g_2 c_W)(N_{i3}^* N_{j3} - N_{i4}^* N_{j4})(\gamma_\mu P_R) \quad (38)$$

where the matrix N is neutralino mixing matrix. Since $\tilde{\chi}_{2,3}^0$ are higgsino-dominated, $m_{\tilde{\chi}_{2,3}^0} \simeq \mu$, thus from Eq.(2.30) we know $N_{i3} : N_{i4} \approx -1$, then $(|N_{i3}|^2 - |N_{i4}|^2) \approx 0$, and $\sigma(pp\rightarrow\tilde{\chi}_i^0\tilde{\chi}_i^0) \approx 0$.

The decay branching ratios of the NLSPs are shown in Fig.1 and Fig.2. From the left plots in Fig.1, we can see that, the chargino $\tilde{\chi}_1^\pm$ decay to $\tilde{\chi}_1^0$ plus a W boson in 100%: when the mass difference between $\tilde{\chi}_1^\pm$ and $\tilde{\chi}_1^0$ is larger than m_W , the W boson is a real one; while when the mass difference is insufficient, the W boson is a virtual one, or the decay is a three-body decay. The low mass difference is negative for us to search for the SUSY particles, since the leptons coming from a virtual W boson are very soft and hard to detect.

The main decay modes of neutralino $\tilde{\chi}_i^0$ ($i=2,3$) are to a $\tilde{\chi}_1^0$ plus a Z boson or a Higgs boson. In the middle and right plots of Fig.1 and in Fig.2, we show the branching ratios of the neutralinos $\tilde{\chi}_i^0$ on the plane of $m_{\tilde{\chi}_i^0}$ vs $m_{\tilde{\chi}_1^0}$, where $i=2,3$. In these plots, we use the dashed line, $m_{\tilde{\chi}_i^0} - m_{\tilde{\chi}_1^0} = m_Z$, and the dotted line, $m_{\tilde{\chi}_i^0} - m_{\tilde{\chi}_1^0} = m_{h_2}$, dividing the plane into 3 parts.

- **Case I:** In the region $m_{\tilde{\chi}_i^0} - m_{\tilde{\chi}_1^0} < m_Z$, the neutralino $\tilde{\chi}_i^0$ can only decay to $\tilde{\chi}_1^0$ plus a virtual Z boson or a light Higgs boson h_1 . And we can see from the lower middle plot of Fig.1 and the upper left plot of Fig.2, the $\tilde{\chi}_2^0$ mainly decay to a virtual Z boson plus a $\tilde{\chi}_1^0$, with only a small fraction to the light Higgs boson h_1 plus $\tilde{\chi}_1^0$. On the contrary, the lower left plot of Fig.2 shows that the $\tilde{\chi}_3^0$ mainly decay to the light Higgs boson h_1 .
- **Case II:** In the region $m_Z \leq m_{\tilde{\chi}_i^0} - m_{\tilde{\chi}_1^0} < m_{h_2}$, the neutralino $\tilde{\chi}_i^0$ can decay to $\tilde{\chi}_1^0$ plus a real Z boson or a light Higgs boson h_1/a_1 . As showed in the upper middle plot of Fig.1, the $\tilde{\chi}_2^0$ mainly decay to a real Z boson plus $\tilde{\chi}_1^0$. While according to the upper right plot of Fig.1 and lower left plot of Fig.2, the $\tilde{\chi}_3^0$ mainly decay to a light Higgs boson h_1 plus $\tilde{\chi}_1^0$.
- **Case III:** In the region $m_{\tilde{\chi}_i^0} - m_{\tilde{\chi}_1^0} \geq m_{h_2}$, all these decay channels are opened. The $\tilde{\chi}_2^0$ mainly decay to $\tilde{\chi}_1^0$ plus a 125 GeV SM-like Higgs boson h_2 , while $\tilde{\chi}_3^0$ mainly decay to $\tilde{\chi}_1^0$ plus Z bosons.

In the channel $\tilde{\chi}_i^0 \rightarrow \tilde{\chi}_1^0 Z$ ($i=2,3$), like the $\tilde{\chi}_1^\pm \rightarrow W^\pm \tilde{\chi}_1^0$, when the mass difference is insufficient the Z boson also becomes a virtual one. In the channel $\tilde{\chi}_i^0 \rightarrow \tilde{\chi}_1^0 H$ ($i=2,3$), where the Higgs boson can be h_1 or h_2 , and h_2 is the SM-like one. Both h_1 and h_2 mainly decay to bb , thus the $t\bar{t}$ background is sizable at the LHC. In the case that Higgs decay to WW, ZZ, or $\tau\tau$, and W or Z decays leptonically, it might contribute to the multilepton final state. Since the light Higgs h_1 is highly singlet-dominated, the $\tilde{\chi}_i^0 \rightarrow \tilde{\chi}_1^0 h_1$ is very hard to contribute to the multilepton signal regions. Thus only the $\tilde{\chi}_i^0 \rightarrow \tilde{\chi}_1^0 h_2$ can contribute to the multilepton signal regions visibly.

It is worth to mention that, when the heavier neutralinos decay to the $\tilde{\chi}_1^0$ LSP, the $\tilde{\chi}_2^0$ and $\tilde{\chi}_3^0$ behave differently. Especially in the case II, $\tilde{\chi}_2^0$ prefers to decay to a Z boson plus $\tilde{\chi}_1^0$, $Br(\tilde{\chi}_2^0 \rightarrow \tilde{\chi}_1^0 Z) > Br(\tilde{\chi}_2^0 \rightarrow \tilde{\chi}_1^0 h_1)$; while $\tilde{\chi}_3^0$ tends to decay to a light Higgs boson h_1 plus $\tilde{\chi}_1^0$, $Br(\tilde{\chi}_3^0 \rightarrow \tilde{\chi}_1^0 Z) < Br(\tilde{\chi}_3^0 \rightarrow \tilde{\chi}_1^0 h_1)$. The couplings $C_{h_1\tilde{\chi}_2^0\tilde{\chi}_1^0}$ and $C_{h_1\tilde{\chi}_3^0\tilde{\chi}_1^0}$ can be written down as

$$C_{h_1\tilde{\chi}_2^0\tilde{\chi}_1^0} \sim \frac{\lambda(N_{14}N_{23} + N_{13}N_{24})S_{13}}{\sqrt{2}} - \sqrt{2}\kappa N_{15}N_{25}S_{13} \quad (39)$$

$$C_{h_1\tilde{\chi}_3^0\tilde{\chi}_1^0} \sim \frac{\lambda(N_{14}N_{33} + N_{13}N_{34})S_{13}}{\sqrt{2}} - \sqrt{2}\kappa N_{15}N_{35}S_{13} \quad (40)$$

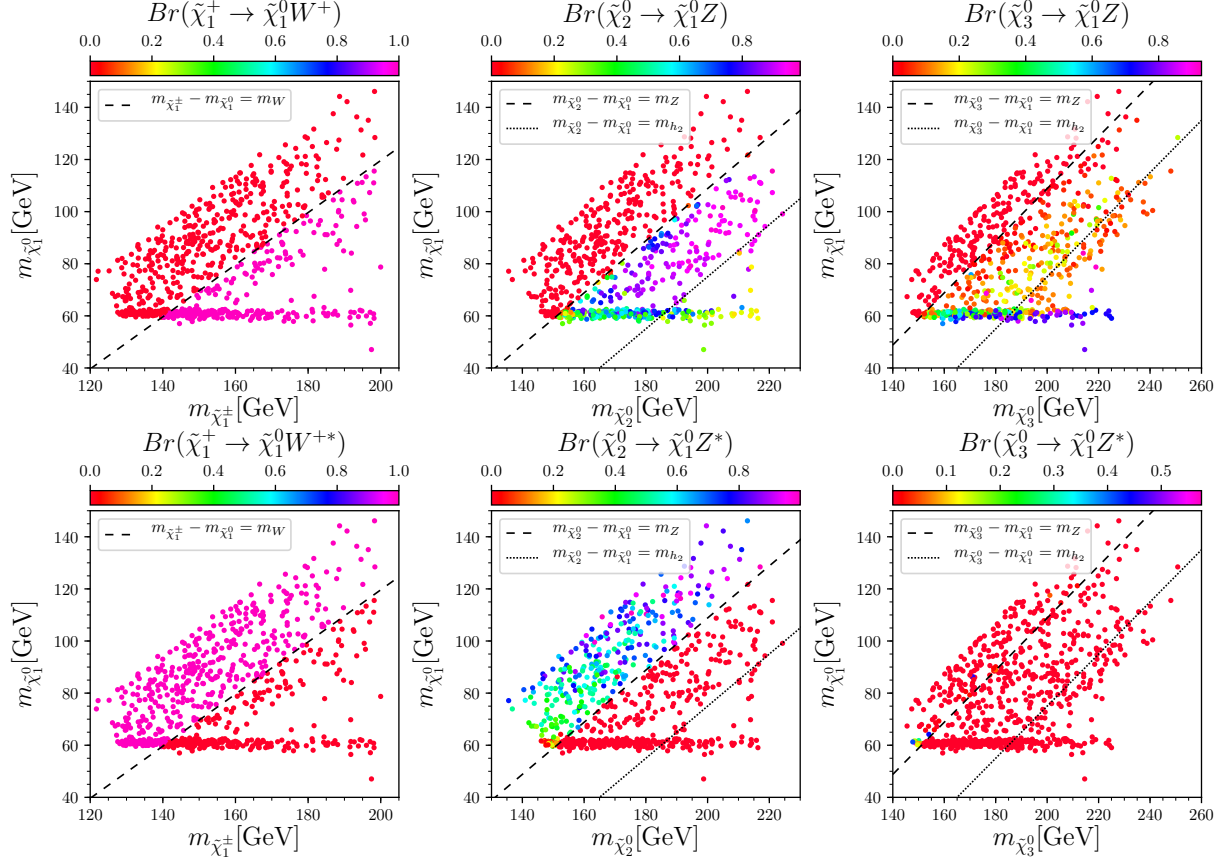


Fig. 1. (color online) The samples in the $m_{\tilde{\chi}_1^0}$ versus $m_{\tilde{\chi}_i^\pm}$ planes (left $i=\pm$, middle $i=2$ and right $i=3$). The colors indicate the branching ratios of the chargino $\tilde{\chi}_1^\pm$ to $\tilde{\chi}_1^0$ plus W boson, and neutralino $\tilde{\chi}_{2,3}^0$ to $\tilde{\chi}_1^0$ plus Z boson respectively. In the upper panel, the W/Z boson is a real one and the decay is real two-body decay; while in the lower panel the W/Z boson is a virtual one and the decay is virtual three-body decay.

where the N_{11} , N_{12} , N_{21} , N_{22} , N_{31} and N_{32} was set to 0 since the wino and bino are very heavy and decoupled in the scNMSSM, and the S_{11} and S_{12} was set to 0 since $|S_{13}| \gg |S_{11}|, |S_{12}|$. $\lambda/\sqrt{2} \ll 1$ and $\sqrt{2}\kappa \ll 1$, so the couplings $C_{h_1\tilde{\chi}_2^0\tilde{\chi}_1^0}$ and $C_{h_1\tilde{\chi}_3^0\tilde{\chi}_1^0}$ are both very small and roughly the same. While the couplings $C_{Z\tilde{\chi}_2^0\tilde{\chi}_1^0}$ and $C_{Z\tilde{\chi}_3^0\tilde{\chi}_1^0}$ can be different from each other according to Eq.(38), which can be approximated to

$$C_{Z\tilde{\chi}_2^0\tilde{\chi}_1^0} \sim \frac{g_2}{c_W} (N_{13}N_{23} - N_{14}N_{24}) \quad (41)$$

$$C_{Z\tilde{\chi}_3^0\tilde{\chi}_1^0} \sim \frac{g_2}{c_W} (N_{13}N_{33} - N_{14}N_{34}) \quad (42)$$

where the $g_2/c_W \sim 1$. When the two terms in Eq.(41) or Eq.(42) have different sign, and do not cancel with each other, the couplings $C_{Z\tilde{\chi}_i^0\tilde{\chi}_1^0}$ can be much larger than $C_{h_1\tilde{\chi}_i^0\tilde{\chi}_1^0}$; otherwise the cancel between the two terms can make $C_{Z\tilde{\chi}_i^0\tilde{\chi}_1^0}$ smaller than $C_{h_1\tilde{\chi}_i^0\tilde{\chi}_1^0}$. For some surviving samples, $C_{Z\tilde{\chi}_3^0\tilde{\chi}_1^0}$ have the cancellation between the two terms, and that leads to small $Br(\tilde{\chi}_3^0 \rightarrow \tilde{\chi}_1^0 Z)$ and large $Br(\tilde{\chi}_3^0 \rightarrow \tilde{\chi}_1^0 h_1)$. Six benchmark points are listed in the Table 1.

3.3 Possibility of discovery at the HL-LHC in the future

In this part, we investigate the possibility of detect electroweakinos at the future High Luminosity LHC (HL-LHC). We adopt the same analysis of multilepton final state by CMS [27], only increasing the integrated luminosity from 35.9 fb^{-1} to 300 fb^{-1} , to see the possibility of discovery in the future. And we evaluate the signal significance by

$$ss = S/\sqrt{B} \quad (43)$$

where S and B are the number of events from signal and background processes respectively.

In Fig.3, we show ss on the planes of $m_{\tilde{\chi}_1^0}$ versus $m_{\tilde{\chi}_1^\pm}$, $m_{\tilde{\chi}_2^0}$ and $m_{\tilde{\chi}_3^0}$ respectively. We can see that most of the samples can be checked at 5σ level when the mass difference between LSP $\tilde{\chi}_1^0$ and NLSPs $\tilde{\chi}_1^\pm, \tilde{\chi}_{2,3}^0$ is sufficient. However, there are still some samples that can not be checked at level above 3 or 5 sigma. The main reason is that the mass spectra is compressed, so that the leptons from the decay of NLSPs are very soft. Because \not{p}_T cut has to be very large at the LHC due to the large back-

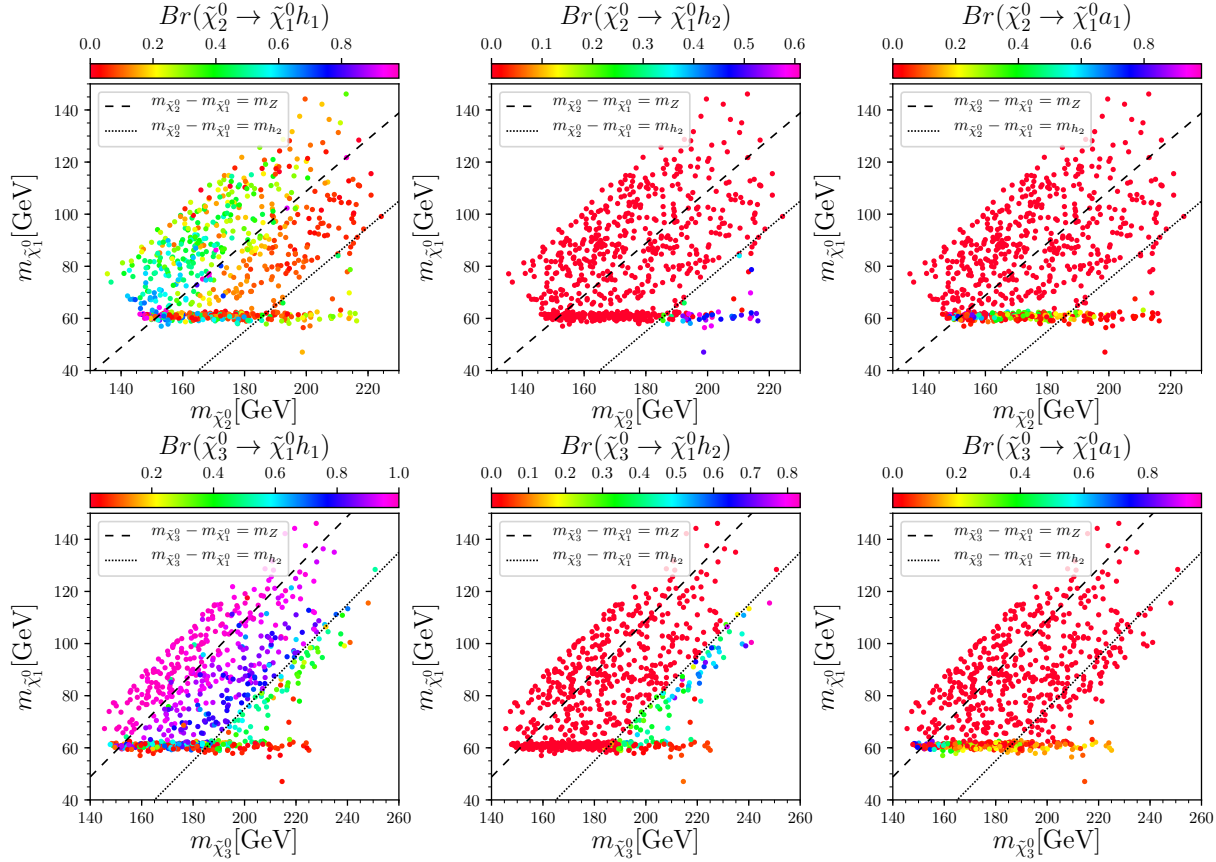


Fig. 2. (color online) The samples in the $m_{\tilde{\chi}_1^0}$ versus $m_{\tilde{\chi}_i^0}$ planes (upper $i=2$, lower $i=3$). From left to the right, colors indicate the branching ratios $Br(\tilde{\chi}_i^0 \rightarrow \tilde{\chi}_1^0 h_1)$, $Br(\tilde{\chi}_i^0 \rightarrow \tilde{\chi}_1^0 h_2)$, and $Br(\tilde{\chi}_i^0 \rightarrow \tilde{\chi}_1^0 a_1)$, respectively. The dashed line and the dotted line means that the mass difference, $m_{\tilde{\chi}_i^0} - m_{\tilde{\chi}_1^0}$, equal to m_Z and m_{h_2} respectively.

Table 1. Masses and branching ratios for 6 benchmark points in the scNMSSM. The signal significances in the last line are calculated with luminosity of 300 fb^{-1} , and with similar analysis of multi-lepton final state as in Ref. [27].

	P1	P2	P3	P4	P5	P6
$m_{\tilde{\chi}_1^\pm}$ (GeV)	183	173	175	189	175	187
$m_{\tilde{\chi}_1^0}$ (GeV)	120	119	103	108	82	92
$m_{\tilde{\chi}_2^0}$ (GeV)	200	187	200	209	202	206
$m_{\tilde{\chi}_3^0}$ (GeV)	216	200	214	216	212	209
$Br(\tilde{\chi}_1^+ \rightarrow \tilde{\chi}_1^0 W)$	0%	0%	0%	100%	100%	100%
$Br(\tilde{\chi}_1^+ \rightarrow \tilde{\chi}_1^0 W^*)$	100%	100%	100%	0%	0%	0%
$Br(\tilde{\chi}_2^0 \rightarrow \tilde{\chi}_1^0 Z)$	0%	0%	90%	93%	94%	95%
$Br(\tilde{\chi}_2^0 \rightarrow \tilde{\chi}_1^0 Z^*)$	80%	65%	0%	0%	0%	0%
$Br(\tilde{\chi}_2^0 \rightarrow \tilde{\chi}_1^0 h_1)$	20%	35%	10%	7%	6%	5%
$Br(\tilde{\chi}_2^0 \rightarrow \tilde{\chi}_1^0 h_2)$	0%	0%	0%	0%	0%	0%
$Br(\tilde{\chi}_3^0 \rightarrow \tilde{\chi}_1^0 Z)$	1%	0%	1%	13%	13%	38%
$Br(\tilde{\chi}_3^0 \rightarrow \tilde{\chi}_1^0 Z^*)$	0%	0%	0%	0%	0%	0%
$Br(\tilde{\chi}_3^0 \rightarrow \tilde{\chi}_1^0 h_1)$	99%	100%	99%	87%	33%	62%
$Br(\tilde{\chi}_3^0 \rightarrow \tilde{\chi}_1^0 h_2)$	0%	0%	0%	0%	54%	0%
$ss = S/\sqrt{B} @ 300 \text{ fb}^{-1} (\sigma)$	3.1	2.9	2.1	3.8	10.8	8.8

ground, detecting soft particles is not easy. Combining with Fig.1 and 2, we can learn the following facts:

- If $\tilde{\chi}_1^\pm$ or $\tilde{\chi}_i^0$ ($i=2,3$) decays to a virtual vector bo-

son, or in the area upon the dashed line in all the plots, the signal significance is less than 5σ , and it is hard to check with 300 fb^{-1} data at the LHC.

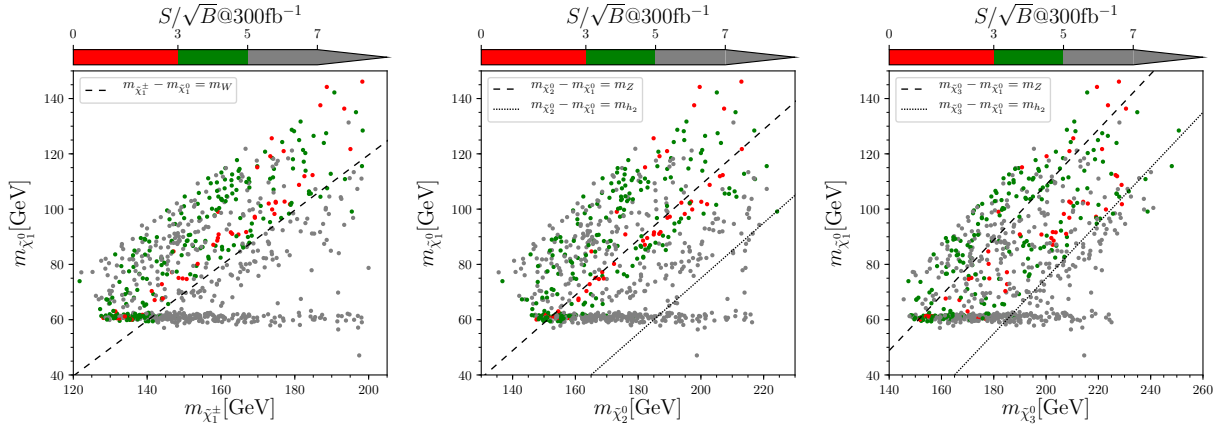


Fig. 3. (color online) The samples in the $m_{\tilde{\chi}_1^0}$ versus $m_{\tilde{\chi}_1^\pm}$ (left), $m_{\tilde{\chi}_1^0}$ versus $m_{\tilde{\chi}_2^0}$ (middle), $m_{\tilde{\chi}_1^0}$ versus $m_{\tilde{\chi}_3^0}$ (right) planes. The colors indicates the signal significance, where red represents $ss < 3\sigma$, green represents $3\sigma < ss < 5\sigma$, and gray represents $ss > 5\sigma$. In the left plane, the dashed line indicates the mass difference equal to m_W , $m_{\tilde{\chi}_1^\pm} - m_{\tilde{\chi}_1^0} = m_W$. In the middle and right planes, the dashed line and dotted line indicate the mass difference equal to m_Z and m_{h_2} respectively, that is, $m_{\tilde{\chi}_i^0} - m_{\tilde{\chi}_1^0} = m_Z$ and $m_{\tilde{\chi}_i^0} - m_{\tilde{\chi}_1^0} = m_{h_2}$, where $i = 2, 3$ for the middle and right planes respectively.

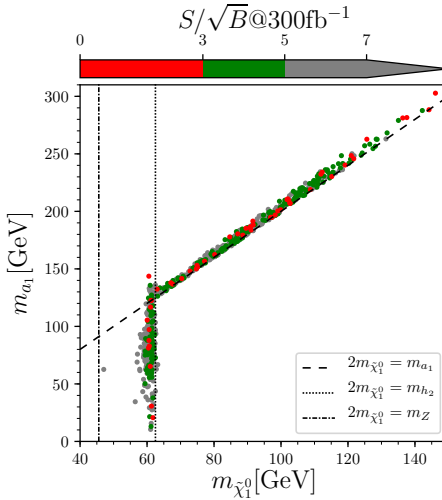


Fig. 4. (color online) The samples in the m_{a_1} versus $m_{\tilde{\chi}_1^0}$ plane. The color convention is the same as in Fig.3. The dashed, dotted and dash-dotted lines indicate $2m_{\tilde{\chi}_1^0}$, equal to m_{a_1} , m_{h_2} , and m_Z respectively.

- If $\tilde{\chi}_1^\pm$ or $\tilde{\chi}_2^0$ decays to a real vector boson, the area between the dashed and dotted line in left and middle plots, the signal significance can be larger than 5σ , and it is easy to check with 300 fb^{-1} data at the LHC.
- The $\tilde{\chi}_3^0$ decay to a light Higgs h_1 , the area between the dashed and dotted line in the right plane, the signal significance is less than 5σ for some samples. The reason is that the light Higgs h_1 mainly decay to $b\bar{b}$, which is hard to distinguish from the background.
- If $\tilde{\chi}_i^0$ ($i = 2, 3$) decays to an SM-like Higgs, or in the area below the dotted line in middle and right

plots, the signal significance is also larger than 5σ for most samples.

For the samples with insufficient mass difference between the NLSPs and LSP, the integrate luminosity 300 fb^{-1} is not enough. So we also tried to increase the luminosity to 3000 fb^{-1} , the result is that nearly all samples can be checked with $ss > 5$ at 3000 fb^{-1} .

In Fig.4, we show the signal significance ss on the planes of $m_{\tilde{\chi}_1^0}$ versus m_{a_1} . We can see that there are mainly two mechanisms for dark matter annihilation: the a_1 funnel where $2m_{\tilde{\chi}_1^0} \simeq m_{a_1}$, and the h_2/Z funnel where $2m_{\tilde{\chi}_1^0} \simeq m_{h_2}$ or $2m_{\tilde{\chi}_1^0} \simeq m_Z$. Unfortunately, searching for the NLSPs is helpless in distinguishing these two mechanisms. While as shown in Ref.[11], the spin-

independent cross section of $\tilde{\chi}_1^0$ can be sizable, so such singlino-dominated dark matter may be accessible in the future direct detections, such as XENONnT and LUX-ZEPLIN (LZ-7 2T).

4 Conclusions

In this work, we have discussed the light higgsino-dominated NLSPs in the scNMSSM, which is also called the non-universal Higgs mass (NUHM) version of the NMSSM. We use the scenario with singlino-dominated $\tilde{\chi}_1^0$ and SM-like h_2 in the scan result in our former work on scNMSSM, where we considered the constraints including theoretical constraints of vacuum stability and Landau pole, experimental constraints of Higgs data, muon g-2, B physics, dark matter relic density and direct searches, etc. In our scenario, the bino and wino are heavy because of the high mass bound of gluino and the unification of gaugino masses at the GUT scale. Thus the $\tilde{\chi}_1^\pm$ and $\tilde{\chi}_{2,3}^0$ are higgsino-dominated and mass-degenerated NLSPs.

We first investigate the direct constraints to these light higgsino-dominated NLSPs, including searching for SUSY particle at the LHC Run-I and Run-II. We use Monte Carlo to do detailed simulations to impose these constraints from search SUSY particles at the LHC. Then we discuss the possibility of checking the light higgsino-dominated NLSPs at the HL-LHC in the future. We use the same analysis by increasing the integrated luminosity to 300 fb^{-1} and 3000 fb^{-1} .

References

- 1 J. E. Kim and H. P. Nilles, Phys. Lett. **138B**, 150 (1984).
- 2 J. Cao, Z. Heng, J. M. Yang and J. Zhu, JHEP **1210** (2012) 079 [arXiv:1207.3698 [hep-ph]].
- 3 J. Cao, Z. X. Heng, J. M. Yang, Y. M. Zhang and J. Y. Zhu, JHEP **1203** (2012) 086 [arXiv:1202.5821 [hep-ph]].
- 4 C. Han, K. i. Hikasa, L. Wu, J. M. Yang and Y. Zhang, Phys. Lett. B **769** (2017) 470 [arXiv:1612.02296 [hep-ph]].
- 5 P. Bechtle *et al.*, Eur. Phys. J. C **76** (2016) no.2, 96 [arXiv:1508.05951 [hep-ph]].
- 6 P. Athron *et al.* [GAMBIT Collaboration], Eur. Phys. J. C **77** (2017) no.12, 824 [arXiv:1705.07935 [hep-ph]].
- 7 K. Kowalska, S. Munir, L. Roszkowski, E. M. Sessolo, S. Trojanowski and Y. L. S. Tsai, Phys. Rev. D **87** (2013) 115010 [arXiv:1211.1693 [hep-ph]].
- 8 J. F. Gunion, Y. Jiang and S. Kraml, Phys. Lett. B **710** (2012) 454 [arXiv:1201.0982 [hep-ph]].
- 9 U. Ellwanger and C. Hugonie, Adv. High Energy Phys. **2012** (2012) 625389 [arXiv:1203.5048 [hep-ph]].
- 10 C. Beskidt, W. de Boer and D. I. Kazakov, Phys. Lett. B **726** (2013) 758 [arXiv:1308.1333 [hep-ph]].
- 11 D. Kim, P. Athron, C. Balazs, B. Farmer and E. Hutchison, Phys. Rev. D **90** (2014) no.5, 055008 [arXiv:1312.4150 [hep-ph]].
- 12 A. Fowlie, Eur. Phys. J. C **74** (2014) no.10, 3105 [arXiv:1407.7534 [hep-ph]].
- 13 D. G. Cerdeño, V. De Romeri, V. Martín-Lozano, K. A. Olive and O. Seto, Eur. Phys. J. C **78** (2018) no.4, 290 [arXiv:1707.03990 [hep-ph]].
- 14 U. Ellwanger, A. Florent and D. Zerwas, JHEP **1101** (2011) 103 [arXiv:1011.0931 [hep-ph]].
- 15 G. Panotopoulos, J. Phys. Conf. Ser. **259** (2010) 012064 [arXiv:1010.4481 [hep-ph]].
- 16 D. E. Lopez-Fogliani, L. Roszkowski, R. Ruiz de Austri and T. A. Varley, Phys. Rev. D **80** (2009) 095013 [arXiv:0906.4911 [hep-ph]].
- 17 G. Belanger, C. Hugonie and A. Pukhov, JCAP **0901** (2009) 023 [arXiv:0811.3224 [hep-ph]].
- 18 A. Djouadi, U. Ellwanger and A. M. Teixeira, JHEP **0904** (2009) 031 [arXiv:0811.2699 [hep-ph]].
- 19 U. Ellwanger, AIP Conf. Proc. **1078** (2009) 73 [arXiv:0809.0779 [hep-ph]].
- 20 C. Hugonie, G. Belanger and A. Pukhov, JCAP **0711** (2007) 009 [arXiv:0707.0628 [hep-ph]].
- 21 D. Das, U. Ellwanger and A. M. Teixeira, JHEP **1304** (2013) 117 [arXiv:1301.7584 [hep-ph]].
- 22 U. Ellwanger and C. Hugonie, JHEP **1408**, 046 (2014)

Finally, we come to the following conclusions regarding the higgsino-dominated $100 \sim 200 \text{ GeV}$ NLSPs in scNMSSM:

- Among the search results for electroweakinos, the ‘multi-lepton final state’ constrain our scenario most, and can exclude some of our samples. While with all data at Run I and up to 36 fb^{-1} data at Run II at the LHC, the search results by ATLAS and CMS can still not exclude the light higgsino-dominated NLSPs of $100 \sim 200 \text{ GeV}$.
- When the mass difference with $\tilde{\chi}_1^0$ is smaller than m_{h_2} , $\tilde{\chi}_2^0$ and $\tilde{\chi}_3^0$ have different preference on decaying to Z/Z^* or h_1 .
- The best channels to detect the NLSPs are through the real two-body decay $\tilde{\chi}_1^\pm \rightarrow \tilde{\chi}_1^0 W$ and $\tilde{\chi}_{2,3}^0 \rightarrow \tilde{\chi}_1^0 Z/h_2$. When the mass difference is sufficient, most of the samples can be checked at 5σ level with future 300 fb^{-1} data at the LHC. While with 3000 fb^{-1} data at the LHC, nearly all of the samples can be checked at 5σ level even if the mass difference is insufficient.
- The a_1 funnel and the h_2/Z funnel are the two main mechanisms for the singlino-dominated LSP annihilating, which can not be distinguished by searching for NLSPs.

We thank Yuanfang Yue, Yang Zhang and Liangliang Shang for useful discussions.

[arXiv:1405.6647 [hep-ph]].

11 K. Wang, F. Wang, J. Zhu and Q. Jie, Chin. Phys. C **42**, no. 10, 103109 (2018) [arXiv:1811.04435 [hep-ph]].

12 W. Abdallah, A. Chatterjee and A. Datta, JHEP **1909**, 095 (2019) [arXiv:1907.06270 [hep-ph]].

D. Das, U. Ellwanger and A. M. Teixeira, JHEP **1204**, 067 (2012) [arXiv:1202.5244 [hep-ph]].

13 A. Pyarelal and S. Su, arXiv:1907.11326 [hep-ph].

14 U. Ellwanger and C. Hugonie, Eur. Phys. J. C **78**, no. 9, 735 (2018) [arXiv:1806.09478 [hep-ph]].

U. Ellwanger, JHEP **1702**, 051 (2017) [arXiv:1612.06574 [hep-ph]].

Q. F. Xiang, X. J. Bi, P. F. Yin and Z. H. Yu, Phys. Rev. D **94**, no. 5, 055031 (2016) [arXiv:1606.02149 [hep-ph]].

M. Badziak, M. Olechowski and P. Szczerbiak, JHEP **1603**, 179 (2016) [arXiv:1512.02472 [hep-ph]].

U. Ellwanger and A. M. Teixeira, JHEP **1410**, 113 (2014) [arXiv:1406.7221 [hep-ph]].

15 U. Ellwanger, JHEP **1311**, 108 (2013) [arXiv:1309.1665 [hep-ph]].

16 F. Domingo, J. S. Kim, V. Martin-Lozano, P. Martin-Ramiro and R. Ruiz de Austri, arXiv:1812.05186 [hep-ph].

17 A. Titterton, U. Ellwanger, H. U. Flaecher, S. Moretti and C. H. Shepherd-Themistocleous, JHEP **1810**, 064 (2018) [arXiv:1807.10672 [hep-ph]].

18 J. S. Kim and T. S. Ray, Eur. Phys. J. C **75**, 40 (2015) [arXiv:1405.3700 [hep-ph]].

B. Dutta, Y. Gao and B. Shakya, Phys. Rev. D **91**, no. 3, 035016 (2015) [arXiv:1412.2774 [hep-ph]].

J. Cao, L. Shang, P. Wu, J. M. Yang and Y. Zhang, Phys. Rev. D **91**, no. 5, 055005 (2015) [arXiv:1410.3239 [hep-ph]].

R. Enberg, S. Munir, C. Prez de los Heros and D. Werder, arXiv:1506.05714 [hep-ph].

C. T. Potter, Eur. Phys. J. C **76**, no. 1, 44 (2016) [arXiv:1505.05554 [hep-ph]].

J. Cao, Y. He, L. Shang, W. Su and Y. Zhang, JHEP **1608** (2016) 037 [arXiv:1606.04416 [hep-ph]].

J. Cao, Y. He, L. Shang, Y. Zhang and P. Zhu, Phys. Rev. D **99** (2019) no. 7, 075020 [arXiv:1810.09143 [hep-ph]].

19 U. Ellwanger, C. Hugonie and A. M. Teixeira, Phys. Rept. **496**, 1 (2010) [arXiv:0910.1785 [hep-ph]].

20 D. J. Miller, R. Nevzorov and P. M. Zerwas, Nucl. Phys. B **681** (2004) 3 [hep-ph/0304049].

21 J. Cao, L. Shang, P. Wu, J. M. Yang and Y. Zhang, JHEP **1510**, 030 (2015) [arXiv:1506.06471 [hep-ph]].

M. Badziak, M. Olechowski and P. Szczerbiak, JHEP **1603**, 179 (2016) [arXiv:1512.02472 [hep-ph]].

22 D. Das, U. Ellwanger and A. M. Teixeira, JHEP **1204**, 067 (2012) [arXiv:1202.5244 [hep-ph]].

W. Abdallah, A. Chatterjee and A. Datta, JHEP **1909**, 095 (2019) [arXiv:1907.06270 [hep-ph]].

23 M. Drees, H. Dreiner, D. Schmeier, J. Tattersall and J. S. Kim, Comput. Phys. Commun. **187**, 227 (2015) [arXiv:1312.2591 [hep-ph]].

J. S. Kim, D. Schmeier, J. Tattersall and K. Rolbiecki, Comput. Phys. Commun. **196**, 535 (2015) [arXiv:1503.01123 [hep-ph]].

D. Derckx, N. Desai, J. S. Kim, K. Rolbiecki, J. Tattersall and T. Weber, Comput. Phys. Commun. **221**, 383 (2017) [arXiv:1611.09856 [hep-ph]].

24 U. Ellwanger and C. Hugonie, Comput. Phys. Commun. **177**, 399 (2007) [hep-ph/0612134].

D. Das, U. Ellwanger and A. M. Teixeira, Comput. Phys. Commun. **183**, 774 (2012) [arXiv:1106.5633 [hep-ph]].

U. Ellwanger, J. F. Gunion and C. Hugonie, JHEP **0502**, 066 (2005) [hep-ph/0406215].

U. Ellwanger and C. Hugonie, Comput. Phys. Commun. **175**, 290 (2006) [hep-ph/0508022].

25 P. Bechtle, O. Brein, S. Heinemeyer, O. Stl, T. Stefaniak, G. Weiglein and K. E. Williams, Eur. Phys. J. C **74**, no. 3, 2693 (2014) [arXiv:1311.0055 [hep-ph]].

26 F. Ambrogi et al, Comput. Phys. Commun., **227**: 72 (2018), arXiv: 1701.06586 [hep-ph]

S. Kraml, S. Kulkarni, U. Laa, A. Lessa, W. Magerl, D. Proschofsky-Spindler, and W. Waltenberger, Eur. Phys. J. C, **74**: 2868 (2014), arXiv: 1312.4175 [hep-ph]

27 [CMS Collaboration], JHEP **1803**, 166 (2018) [arXiv:1709.05406 [hep-ex]].

[CMS Collaboration], JHEP **1803**, 160 (2018) [arXiv:1801.03957 [hep-ex]].

28 The ATLAS collaboration [ATLAS Collaboration], ATLAS-CONF-2016-096.

29 [CMS Collaboration], CMS-PAS-SUS-16-025.

30 [CMS Collaboration], Phys. Lett. B **782** (2018) 440 [arXiv:1801.01846 [hep-ex]].

[ATLAS Collaboration], ATLAS-CONF-2016-013, ATLAS-CONF-2016-050, ATLAS-CONF-2016-054, ATLAS-CONF-2016-076, ATLAS-CONF-2015-082, arXiv:1712.08119, arXiv:1712.02332, arXiv:1709.04183, arXiv:1708.07875, arXiv:1706.03731

31 J. Alwall *et al.*, JHEP **1407**, 079 (2014) [arXiv:1405.0301 [hep-ph]].

32 W. Beenakker, R. Hopker and M. Spira, hep-ph/9611232.

33 T. Sjstrand *et al.*, Comput. Phys. Commun. **191**, 159 (2015) [arXiv:1410.3012 [hep-ph]].

34 [DELPHES 3 Collaboration], JHEP **1402**, 057 (2014) [arXiv:1307.6346 [hep-ex]].

35 M. Cacciari, G. P. Salam and G. Soyez, JHEP **0804**, 063 (2008) [arXiv:0802.1189 [hep-ph]].

36 [ATLAS Collaboration], arXiv:1912.08479 [hep-ex].

[ATLAS Collaboration], ATLAS-CONF-2019-020.

37 C. G. Lester and D. J. Summers, Phys. Lett. B **463**, 99 (1999) [hep-ph/9906349].

A. Barr, C. Lester and P. Stephens, J. Phys. G **29**, 2343 (2003) [hep-ph/0304226].

H. C. Cheng and Z. Han, JHEP **0812**, 063 (2008) [arXiv:0810.5178 [hep-ph]].

Y. Bai, H. C. Cheng, J. Gallicchio and J. Gu, JHEP **1207**, 110 (2012) [arXiv:1203.4813 [hep-ph]].

38 [ATLAS Collaboration], arXiv:1908.08215 [hep-ex].

[ATLAS Collaboration], ATLAS-CONF-2019-008.

[ATLAS Collaboration], ATLAS-CONF-2019-014.

[CMS Collaboration], Phys. Lett. B **782**, 440 (2018) [arXiv:1801.01846 [hep-ex]].

[ATLAS Collaboration], ATLAS-CONF-2019-018.

[CMS Collaboration], CMS-PAS-SUS-18-006.

39 S. Buddenbrock *et al.*, JHEP **1910** (2019) 157 [arXiv:1901.05300 [hep-ph]].

S. von Buddenbrock *et al.*, Eur. Phys. J. C **76** (2016) no.10, 580 [arXiv:1606.01674 [hep-ph]].

S. von Buddenbrock *et al.*, J. Phys. G **45** (2018) no.11, 115003 [arXiv:1711.07874 [hep-ph]].

40 [ATLAS Collaboration], ATLAS-CONF-2019-019.

[CMS Collaboration], CMS-PAS-SUS-18-007.

41 [ATLAS Collaboration], Phys. Rev. D **100**, no. 1, 012006 (2019) [arXiv:1812.09432 [hep-ex]].

42 [ATLAS Collaboration], arXiv:1909.09226 [hep-ex].

43 [ATLAS Collaboration], arXiv:1911.12606 [hep-ex].

[CMS Collaboration], arXiv:1910.01185 [hep-ex].